

## Original Research Article

# Quinazoline Derivatives as Corrosion Inhibitors on Aluminium Metal Surface: A Theoretical Study

Fater Iorhuna , Adulfatah Shehu Muhammad , Abdullahi Muhammad Ayuba\*

Department of Pure and Industrial Chemistry, Faculty of Physical Sciences, Bayero University, Kano, Nigeria

## ARTICLE INFO

## Article history

Submitted: 13 November 2022

Revised: 15 December 2022

Accepted: 17 December 2022

Available online: 18 December 2022

Manuscript ID: [AJCA-2211-1347](#)

Checked for Plagiarism: Yes

DOI: [10.22034/AJCA.2023.370123.1347](https://doi.org/10.22034/AJCA.2023.370123.1347)

## KEYWORDS

Adsorption

Quantum chemical parameters

Molecular dynamic simulation

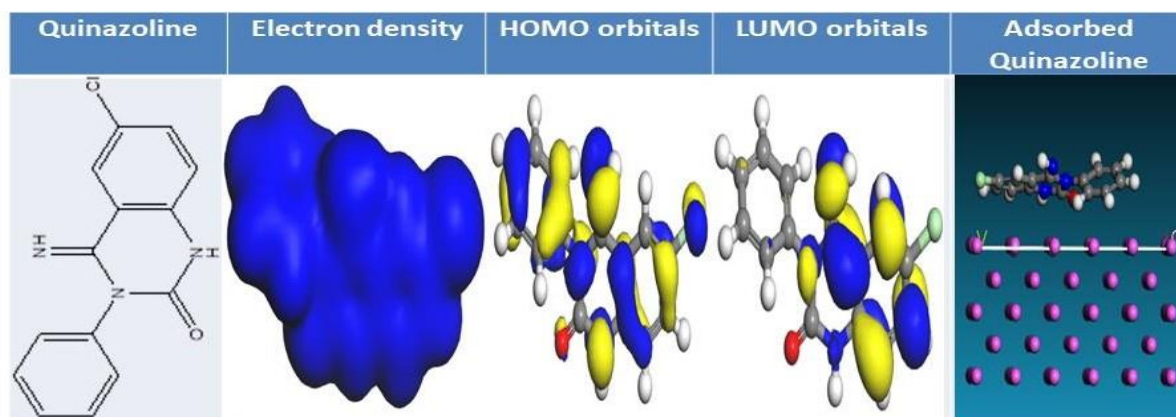
Fukui indices

Van der Waals

## ABSTRACT

Quantum chemical calculations and molecular dynamics simulation techniques were used to assess the corrosion inhibition potential of the compound quinazoline (QZN) and two of its derivatives, 6-chloro-4-imino-3-phenyl-3,4-dihydro-1H quinazoline-2-thione (QZT) and 6-chloro-4-imino-3-phenyl-3,4-dihydro-1H quinazoline-2-one (QZO). The values of the quantum chemical parameters  $E_{HOMO}$ ,  $E_{LUMO}$ , energy gap ( $\Delta E$ ), the energy of back donation ( $\Delta E_{b-d}$ ), dipole moment ( $\mu$ ), electronegativity ( $\chi$ ), global hardness ( $\eta$ ), global electrophilicity index ( $\omega$ ), nucleophilicity ( $\epsilon$ ) and others were determined. The quantum chemical parameters calculated revealed that QZO is relatively more nucleophilic in nature and potentially a better inhibitor. The Fukui indices values discovered that the hetero atoms (N, O and S) of the studied compounds are responsible for their inhibitive characteristics. According to the calculated binding and adsorption energies obtained from the quenched molecular dynamic simulations, the relatively low values obtained of less than 100 kcal/mol results in the molecules being weakly adsorbed onto the surface of Al(1 1 0) through van der Waals forces and consequently obey the physical adsorption mechanism in the order: QZO>QZT> QZN. The examined molecules' varied bond lengths and angles before and after adsorption on the Al(1 1 0) surface demonstrate the nature of adsorption and the molecules' non-planarity on the surface of the metal. QZO and QZT have larger molecular sizes and additional hetero atoms (O and S), making them possibly more corrosion-inhibitive on Al(1 1 0) surfaces than QZN.

## GRAPHICAL ABSTRACT



\* Corresponding author: Ayuba, Abdullahi Muhammad

✉ E-mail: [ayubaabdullahi@buk.edu.ng](mailto:ayubaabdullahi@buk.edu.ng)

© 2023 by SPC (Sami Publishing Company)

## Introduction

Despite being a precious material in construction and other industries, aluminum is vulnerable to corrosion in hostile environments. Thus, it must be safeguarded [1,2]. Metals become susceptible to corrosion when hydrochloric acid solutions are used for cleaning, pickling, oil well acidization and acid descaling [3]. Due to the production of an amphoteric protective oxide covering on its surface upon contact with the environment or aqueous solutions, aluminum has the extraordinary property of being reasonably resistant to corrosion [4]. It can still corrode in highly corrosive or aggressive environments [1]. Due to its great technological value and numerous industrial and household applications, corrosion protection of this metal has been a topic of significance [5].

Recently, most structural failures have been linked to the materials used, most notably those in which aluminum are either the primary metal or a significant component (alloy) [6]. Therefore, it is necessary to lessen or eliminate this threat by using inhibitors to stop the metal from degrading in the environment [7].

In this regard, organic chemicals have found extensive usage as corrosion inhibitors, but the majority of them are expensive and unfriendly to the environment [1-3,6]. Therefore, natural products with a plant origin are recognized as readily available, affordable and environmentally beneficial, making them viable inhibitors. Plant extracts from the leaves, bark and roots are considered environmentally safe since they work as compounds that prevent the corrosion of metals and their alloys in various conditions [8]. Numerous earlier investigations demonstrated that naturally occurring compounds with a plant origin can effectively be used as a metal corrosion inhibitor. Most inhibitor compounds derived from plants contain hetero atoms,

including O, N, S and P, which are said to improve adsorption and inhibitory effectiveness [9-11].

The identification and evaluation of inhibitor potentials and process mechanisms were made simpler by the advent of computer-based programs to address corrosion issues. Most recently, attention has been focused on the utilization of the quantum chemical parameters and molecular dynamic simulation approaches to examine the inhibitory potentials of some of these phytochemicals [12].

In the current investigation, the established phytochemicals from *Sarcocephalus latifolius* leaves, quinazoline compound and some of its derivatives were employed to examine their ability to prevent the corrosion of aluminum metal surfaces. Theoretically, this was accomplished by computing quantum chemical parameters and simulating the motion of quinazolines on aluminum using molecular dynamics. The structures of the investigated compounds are demonstrated in Figure 1.

## Computational Methods

### *Sketching and Geometric Optimization of the Quinazolines*

ChemDraw Ultra 7.0.3 CambridgeSoft was used to create sketches of the investigated compounds. Each molecular structure needs to be optimized once it has been constructed to bring it to a stable configuration. The atoms' coordinates are changed iteratively during this process to bring the structure's energy to a stationary point or where the forces acting on the atoms are zero. During the energy reduction, a relative minimum on the energy hypersurface was sought after. It is anticipated that the geometry corresponding to this structure will closely resemble the system's real physical structure when it is in equilibrium [11]. The molecules' torsional and conformational energies were reduced using DMol<sup>3</sup> optimization, a feature of BIOVIA Materials Studio 8.0.

(Accelrys, Inc.). The compounds were imported from ChemDraw into Materials Studio. The optimization process was carried out using the following settings: DFT-D with a restricted spin polarization DNP+ basis. The local density functional was set to B3LYP in the gaseous phase [2,11,13].

#### Quantum Chemical Parameters Calculations

The quantum chemical calculations based on Density Functional Theory (DFT) were performed using the DMol<sup>3</sup> package in the BIOVIA Material studio 8.0 (Accelrys, Inc.). The B3LYP functional with the "double-numeric plus polarization" (DNP) basis set in the gaseous phase model was used to calculate the parameters. To identify the active sites and determine the local and global reactivities of the compounds in connection to corrosion inhibition, the total electron density, distribution of Frontier molecular orbitals ( $E_{HOMO}$  and  $E_{LUMO}$ ) and Fukui indices were evaluated.

Using Koopman's theorem, global parameters such as electronegativity ( $\chi$ ), hardness ( $\eta$ ), softness ( $\sigma$ ), global electrophilicity index ( $\omega$ ), nucleophilicity ( $\varepsilon$ ), the energy of back donation ( $\Delta E_{b-d}$ ), fraction of electron(s) transfer ( $\Delta N$ ) and local parameters such as the Fukui function  $f(r)$  were evaluated. Ionization energy (IP), electron affinity (EA) and other chemical reactivity descriptors were also calculated. Such computations were performed using Equations 1-10:

$$IE: \text{ Ionization energy (eV) } IE = -E_{HOMO} \quad (1)$$

$$AE: \text{ Electron affinity (eV) } AE = -E_{LUMO} \quad (2)$$

$$\Delta E: \text{ Energy gap (eV) } \Delta E_g = E_{LUMO} - E_{HOMO} \quad (3)$$

$$\chi: \text{ Absolute electronegativity (eV)}$$

$$\chi = \frac{I+A}{2} = -\frac{1}{2}(E_{HOMO} + E_{LUMO}) \quad (4)$$

$$\eta: \text{ Global hardness } \eta = \frac{I-A}{2} = \frac{E_{LUMO} - E_{HOMO}}{2} \quad (5)$$

$$\sigma: \text{ Global softness } \sigma = -\frac{2}{E_{HOMO} - E_{LUMO}} \quad (6)$$

$$\omega: \text{ Global electrophilicity index } \omega = \frac{\mu^2}{2\eta} = \frac{\chi^2}{2\eta} \quad (7)$$

$$\varepsilon: \text{ Nucleophilicity } \varepsilon = \frac{1}{\omega} \quad (8)$$

$$\Delta E_{b-d}: \text{ Energy of back donation}$$

$$\Delta E_{b-d} = -\frac{\eta}{4} = \frac{1}{8}(E_{HOMO} - E_{LUMO}) \quad (9)$$

$$\Delta N: \text{ Fraction of electron(s) transferred}$$

$$\Delta N = \frac{\chi_{Al} - \chi_{inh}}{2(\eta_{Al} + \eta_{inh})} \quad (10)$$

Where  $\eta_{Al}$  and  $\eta_{inh}$  stand for the absolute hardness of Al and the inhibitor molecule, whereas  $\chi_{Al}$  and  $\chi_{inh}$  stand for the absolute electronegativity of Al and the inhibitor molecule, respectively. Assuming that for a metallic bulk IP = EA because they are softer than the neutral metallic atoms, the electronegativity of the inhibitor ( $\chi_{inh}$ ) is assumed to be equal to 0 eV, the electronegativity of the bulk aluminum is calculated to be  $\chi = 5.60$  eV and its global hardness  $\eta_{Al} = 0$  [1, 11, 14-15].

Another global descriptor is the dual descriptor  $\Delta f(k)$ , or second order Fukui function ( $f^2$ ) given in equations 11-14. It is described as being different from electrophilic and nucleophilic Fukui functions. Site k favours a nucleophilic assault if  $f^2(r) > 0$ , whereas site k prefers an electrophilic attack if  $f^2(r) < 0$ . This suggests that  $f^2(r)$  functions as a selectivity index for nucleophilic or electrophilic assaults of an entire molecule.

For nucleophilic attack:

$$f(k)^+ = qk(N+1) - qk(N) \quad (11)$$

For electrophilic attack:

$$f(k)^- = qk(N) - qk(N-1) \quad (12)$$

For radical attack:

$$f(k)^0 = \frac{qk(N+1) - qk(N-1)}{2} \quad (13)$$

Second order Fukui function:

$$\Delta f(r) = f^+ - f^- = f^2 \quad (14)$$

Where  $q_k$  represents the electron density at a point r in space around the molecule or the gross charge of atom k in the molecule. The molecule's total number of electrons is denoted by the letter N. With the addition of an electron to the LUMO

of the neutral molecule, N+1 represents an anion: N-1 corresponds to the cation in which the neutral molecules' HOMO has had an electron removed. The ground state geometry served as the basis for all calculations. Using an atomic charge partitioning scheme, such as Mulliken population analysis in equations 11–14, these functions were condensed to the nuclei [1,11,14,15].

### Molecular Dynamic Simulations

The Al(1 1 0) surface, which is comparatively the most stable and densely packed with atoms, was used to model each system. The BIOVIA Material Studio 8.0 software's FORCITE tools, which are part of the simulation, were used to carry out the process. A representative portion of the surface was modeled using calculations utilizing the COM-PASS force field and Smart algorithm in a simulation box measuring 17 Å by 12 Å by 28 Å with a periodic boundary condition. The aluminum crystal was split with a fractional depth of 3.0 Å along the (1 1 0) plane. Before optimizing the surfaces and enlarging them into a 5 x 5 supercell to prevent edge effects by suitably accommodating the examined molecule, the geometry of the bottom layers was restricted.

A trade-off between a system with too much kinetic energy, where the molecule desorbs from the surface and a system with insufficient kinetic energy, where the molecule cannot move across

the surface, was represented by the fixed temperature at 350K. The NVE (microcanonical) ensemble was used to set the temperature, with a time step of 1fs and a simulation time of 5ps. To achieve a maximum of 20 quench cycle configurations, the system was configured to quench every 250 steps. To acquire the various interactions of the molecule with the surfaces, FOR-CITE optimized structures of the molecules and surfaces were employed [1,2,14].

Al(1 1 0) was created for simulations with a surface that was larger than the size of the molecules needed to fit on it and optimally sized to prevent edge effects of ghost molecules that could affect the calculations [1-2, 14]. Using the expression provided in equation 15, the adsorption energy between each inhibitor molecule and the Al(1 1 0) surface was computed.

$$E_{\text{Adsorption}} = E_{\text{total}} - (E_{\text{inhibitor}} + E_{\text{Al surface}}) \quad (15)$$

Where  $E_{\text{Adsorption}}$  is the adsorption energy,  $E_{\text{total}}$  is the total energy of the molecule and the Al(1 1 0) surface,  $E_{\text{inhibitor}}$  is the energy of the inhibitor molecule alone and  $E_{\text{Al surface}}$  is the energy of the Al (1 1 0) surface only [16].

The binding energy of the compound on the Al(1 1 0) surface is given by equation 16:

$$E_{\text{binding}} = - E_{\text{adsorption}} \quad (16)$$

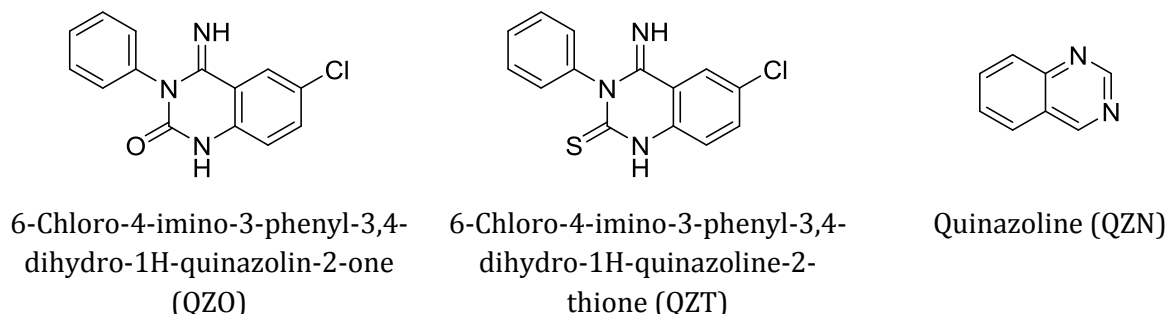


**Figure 1.** Molecular structure of the studied quinazolines

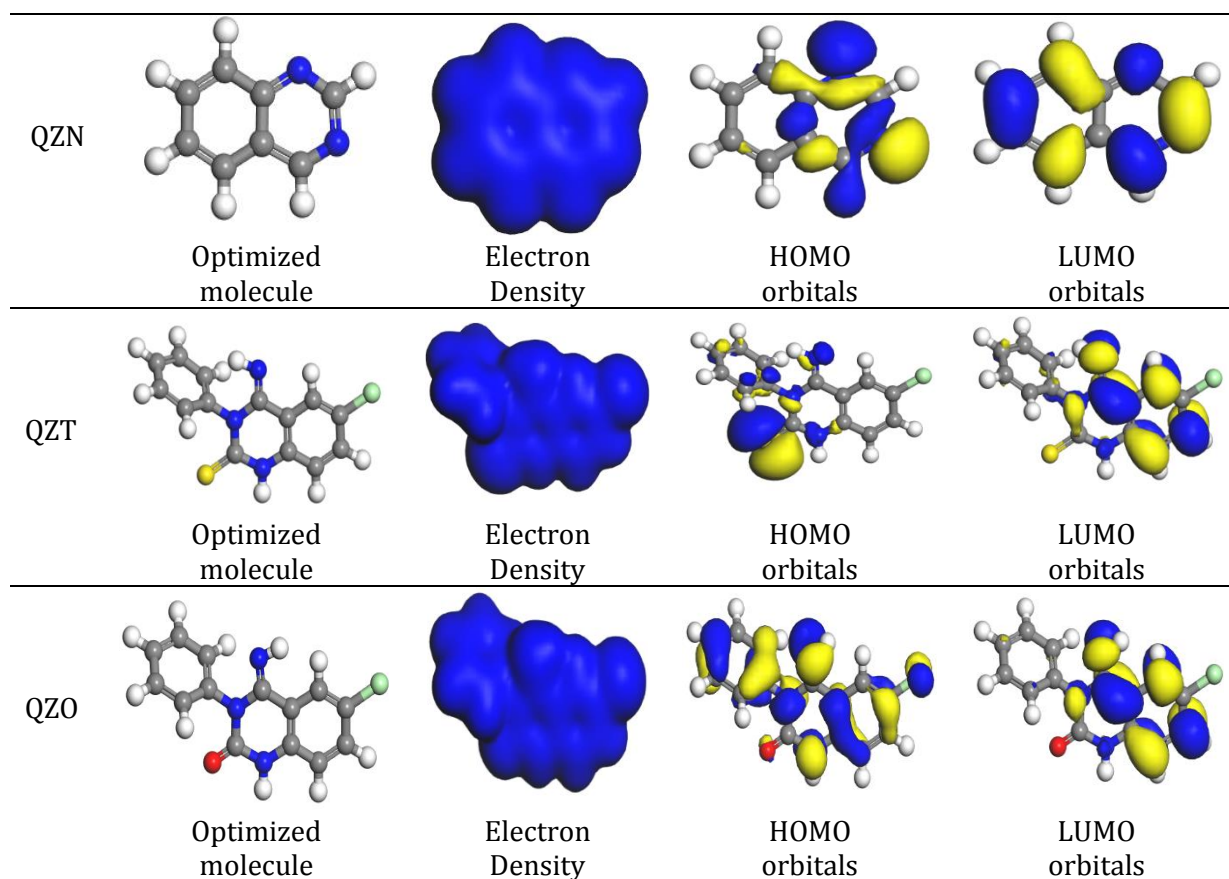
## Results and discussion

### Quantum Chemical Calculations

#### Frontier molecular orbitals

The electrical characteristics of the inhibitors, including electron density and partial charges (pi-bonds) on the atoms, among others, determine how reactive they are [17,18]. Quantum chemical computations may be used to get these features. The selectivity of the compounds utilized as inhibitors is crucial information that this method provides for understanding corrosion-related issues [19]. Figure 2 shows the molecules under study's

optimal structure, total electron density, HOMO orbitals and LUMO orbitals. The molecules' total electron density suggested that the entire molecule could improve corrosion inhibition on metal surfaces during the inhibition phase [1, 20]. The quinazoline and its derivatives' functional groups comprised of hetero atoms like nitrogen, oxygen and chlorine (QZO), sulfur, nitrogen and chlorine (QZT) and nitrogen (QZN), respectively, which are crucial for the suppression of metal corrosion. The HOMO orbitals are discovered to surround the thiol functional group in QZT, the amine functional group in QZN and the halogen atom in QZO, respectively. All the compounds under study had LUMO orbitals centered on the benzene  $\pi$ -bonds.



Key: The grey atom represents Carbon, white represents Hydrogen, yellow represents Sulphur, green represents nitrogen and light blue represents Chlorine atom.

**Figure 2.** Total electron density and Frontier orbitals of the quinazolines

### Quantum chemical properties

$E_{\text{HOMO}}$ ,  $E_{\text{LUMO}}$ , energy gap ( $\Delta E_g$ ), dipole moment ( $\mu$ ), electronegativity ( $\chi$ ), global hardness ( $\eta$ ), global softness ( $\sigma$ ), global electrophilicity index ( $\omega$ ), nucleophilicity ( $\epsilon$ ), the energy of back donation ( $\Delta E_{\text{b-d}}$ ) and the fraction of electron(s) ( $\Delta N$ ) transferred from each molecule to the study metal are among the quantum chemical properties assessed from the study of these molecules. These quantum characteristics reveal the metal inhibition potentials of the inhibitor compounds [11,21]. The calculated parameters are shown in Table 1 as they are.

The lowest unoccupied molecular orbital energy ( $E_{\text{LUMO}}$ ) is typically associated with the level at which electrons are accepted by the molecule from the p/d-orbitals of the aluminium metal surface. In contrast, the highest occupied molecular orbital energy ( $E_{\text{HOMO}}$ ) predicts the reactivity potential of the molecule to donate electrons to the empty p/d-orbitals of the metal surface of Aluminium (Al). These variables are reliable tools required for forecasting electron donation ( $E_{\text{HOMO}}$ ) and acceptance ( $E_{\text{LUMO}}$ ) abilities in a molecule. The energy that must be overcome before an electron may go from the HOMO level to the LUMO level is known as the energy gap ( $\Delta E_g$ ), which is the difference between  $E_{\text{LUMO}}$  and  $E_{\text{HOMO}}$ .

The easier it is for electrons to transition from the HOMO level to the LUMO level in a molecule, the lower the energy gap of the molecule [1-5]. Based on the values of the energy gaps,  $\Delta E_g$  for the various compounds and, therefore, the inhibition potentials, the order of the molecule's electron transfer potential in this work is QZO>QZN>QZT.

This is a clear indicator that the efficiency of the molecules is mostly through electron transfer because the number of electrons transferred ( $\Delta N$ ) from each molecule to the Aluminium (Al) surface is positive and smaller than 3.6 [22-23]. The molecule with the highest  $\Delta N$  content has the

potential to be the most effective at inhibiting corrosion. In the compounds under investigation, QZT has the highest  $\Delta N_{\text{Al}}$  value (0.809). The compounds' ionization energy and electron affinities fall within the range of some of the values published for top corrosion inhibitors [23-25].

The global softness is the opposite of the global hardness, which demonstrates how easily molecules may absorb electrons from the Al surface. The global hardness confirmed how easily the electrons could donate values to the p-orbital of the aluminum [26-27]. The values of the molecules' dipole moment explain the molecules' polarity (debye). The molecules' dipole moments are in the following order: QZO>QZN>QZT, indicating that the molecule with the most significant charge separation has the lowest stability; however, the most reactivity, allowing it to donate electrons more efficiently than the other molecules [28].

Another crucial factor that explains the interaction of inhibitor molecules with metal surfaces is the energy of back donation or  $\Delta E_{\text{b-d}}$ . Gomez *et al.* [29] proposed the back donation procedure. Bedair [30] encourages back donating when the global hardness value is positive and the  $\Delta E_{\text{b-d}}$  value is negative. According to Umaru and Ayuba [31], the interaction between the inhibitor molecules and the aluminum surface involves the transfer of charge from the inhibitor molecules to the aluminum metal and vice versa. Table 1's global hardness values for both molecules are positive, while the back donation values are negative. Based on the energy of back donation data, the molecules' inhibitory efficiency follows the QZO>QZN>QZT, which is consistent with the previously discussed parameters.

The ability of molecules to receive electrons is indicated by their electrophilicity index ( $\omega$ ). Still, their inclination to donate or share electrons is shown by their nucleophilicity index ( $\epsilon$ ), which is the inverse of electrophilicity ( $1/\omega$ ) [31]. It is



well recognized that whereas compounds with high nucleophilicity values are suitable corrosion inhibitors, those with high electrophilicity index values are not [32]. Due to the high reliance of the B3LYP functional on electronegativity, Table 1 reported large values for the electrophilicity index of the molecules. As a result, these two parameters cannot be used to infer any sequence about the inhibition efficiency of the studied molecules, as suggested by Guo *et al.* [32].

**Table 1.** Quantum chemical parameters of the molecules

Properties	QZN	QZT	QZO
$E_{\text{HOMO}}$ (eV)	-5.205	-4.767	-5.303
$E_{\text{LUMO}}$ (eV)	-2.190	-2.080	-2.215
$\Delta E_g$ (eV)	-3.015	-2.687	-3.088
$\mu$ (Debye)	2.110	2.100	2.112
IE (eV)	5.205	4.767	5.303
AE (eV)	2.190	2.080	2.215
$\chi$ (eV)	3.698	3.424	3.759
$\eta$ (eV)	1.508	1.345	1.544
$\sigma$ (eV) <sup>-1</sup>	0.663	0.743	0.648
$\omega$ (eV)	4.534	4.358	4.576
$\varepsilon$ (eV) <sup>-1</sup>	0.221	0.229	0.219
$\Delta E_{\text{b-d}}$ (eV)	-0.377	-0.336	-0.386
$\Delta N$	0.631	0.809	0.596

#### Fukui Functions

By choosing the region where the reaction is most likely to occur by either giving or taking electrons, molecules' local reactivity increases

molecules' reactivity during electron transfer [11]. A molecule's point of attack is indicated by the nucleophilic Fukui function ( $f^+$ ), the electrophilic Fukui function ( $f^-$ ) and the radical Fukui function ( $f^0$ ) [9]. Only the nucleophilic ( $f^+$ ) and electrophilic ( $f^-$ ) Fukui functions were examined in this work and the results of those with the highest values are shown in Table 2. The HOMO and LUMO orbitals are represented by the electrophilic and nucleophilic Fukui functions, respectively.

The reaction's mechanism predicted that electrons would transition from HOMO to LUMO orbitals during adsorption in preparation for potential bond formation [7-9]. According to the results in Table 2, the thionic functional group at S<sub>11</sub>, where QZT has the most excellent values of ( $f^+$ ) and ( $f^-$ ), is also where QZN, the reference molecule, has the highest Eigenvalues for both nucleophilic and electrophilic attack, occurs. For both nucleophilic and electrophilic attacks on the molecule, the aryl-halide functional group (Cl<sub>19</sub>) on the QZO molecule displayed the most significant Eigenvalues (Figure 3).

When nucleophilic and electrophilic attacks are made on the same atom in molecules, the molecule's most outstanding Eigenvalues indicate that this atom has the highest level of reactivity [11]. The nucleophilic and electrophilic assaults on the surface of Al during the metal's corrosion inhibition process might be attributed to the heteroatoms nitrogen, sulfur and chlorine present in their structures.

**Table 2.** Fukui function parameters of the studied molecule

Compound	Atom	Nucleophilic attack ( $f^+$ )		Electrophilic attack ( $f^-$ )	
		Mulliken	Hirshfeld	Mulliken	Hirshfeld
QZN	N <sub>3</sub>	0.100	0.096	0.273	0.191
QZT	S <sub>11</sub>	0.149	0.106	0.365	0.403
QZO	Cl <sub>19</sub>	0.104	0.086	0.102	0.099

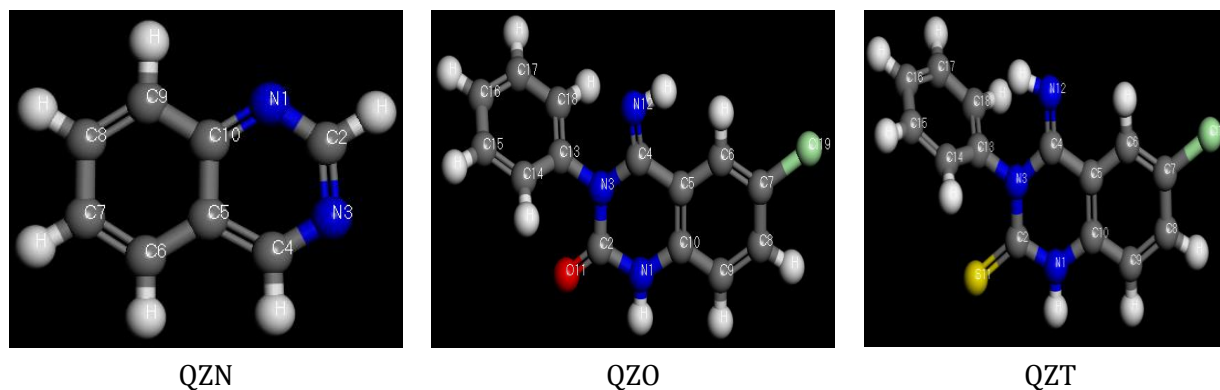


**Figure 3.** Labeled atoms of the studied molecules

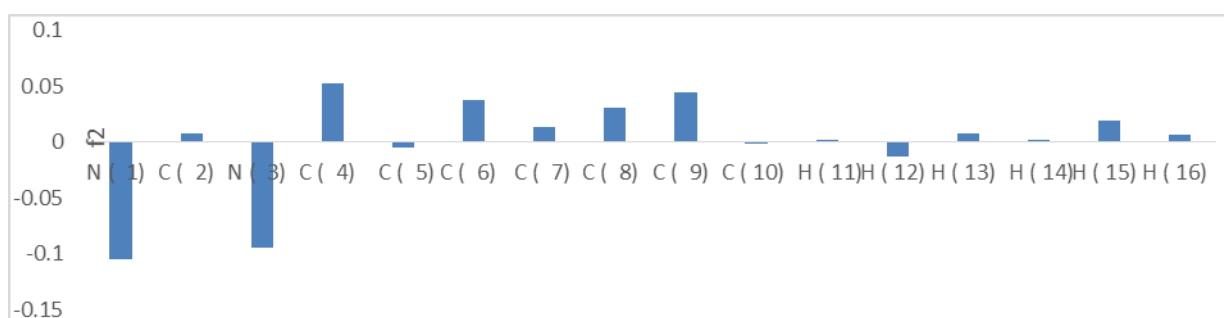


**Figure 4a.** Graphical representation of Fukui function for QZN

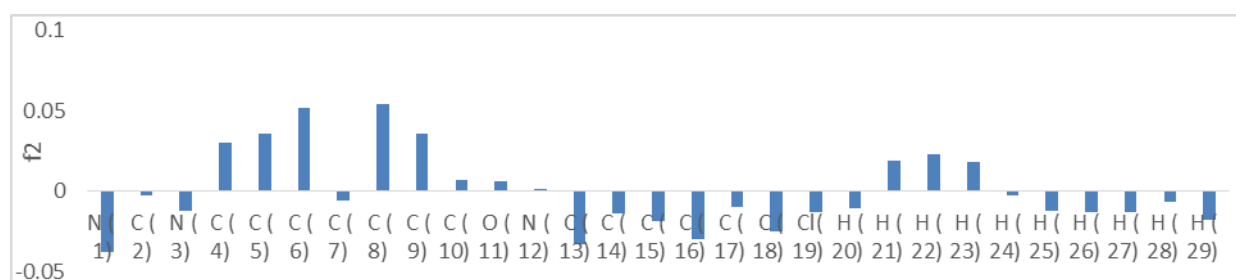


**Figure 4b.** Graphical representation of Fukui function for QZT

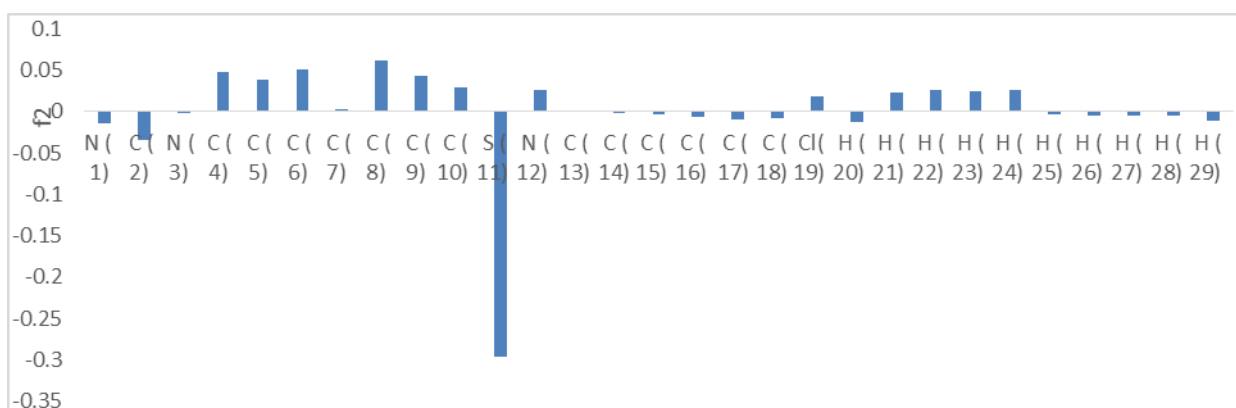


**Figure 4c.** Graphical representation of Fukui function for QZO



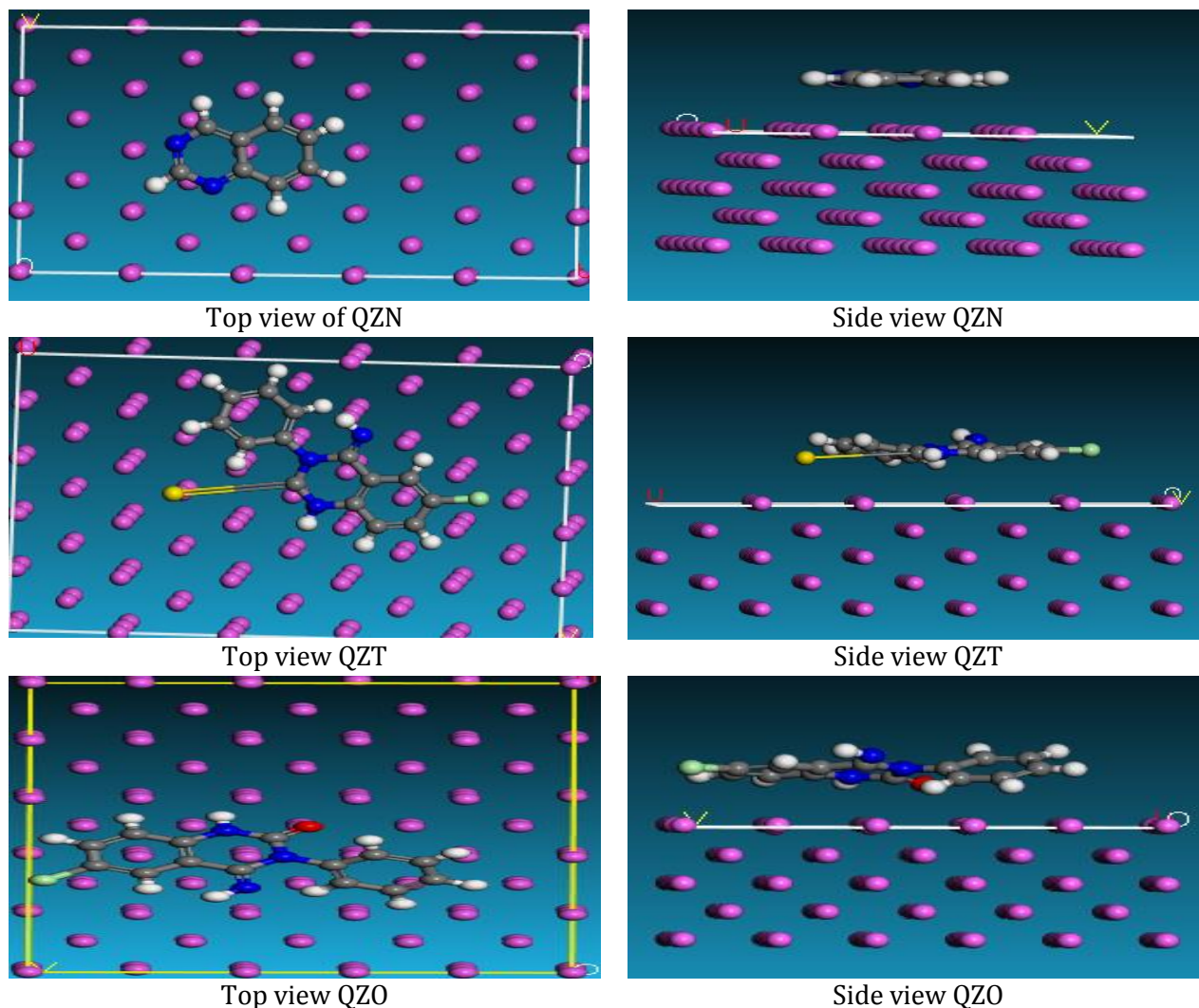


**Figure 5.** The snapshot of adsorbed molecules on the Al(1 1 0) surface

Another crucial local reactivity parameter is the second-order Fukui function ( $f^2$ ). The computed values of the second-order Fukui functions are shown graphically in Figures 4a, b and c and in Table 3. With the help of these illustrations and Table 3, it is possible to see that in QZO, 68.75% of the elements in Figure 4a exhibit positive values of second-order Fukui functions ( $f^2 > 0$ ), whereas 31.25% of the elements exhibit negative values ( $f^2 < 0$ ). According to these values for QZT, 62.07% of the items in Figure 4b showed positive values for second-order Fukui functions, while 37.93% showed negative values. Figure 4c and Table 3 show the Fukui second function for QZN, which has  $f^2 > 0$  percentages of 55.17% and  $f^2 < 0$

percentages of 44.83%. This leads to the conclusion that QZO is more nucleophilic than QZT and QZN and, as a result, more effective at preventing the corrosion of aluminum metal surface [32]. The order of inhibitory effects, in this case, is QZO>QZT>QZN.

**Table 3.** Percent second Fukui function of the Studied Molecules

Molecule	F <sup>2+</sup> %	F <sup>2-</sup> %
QZO	68.75	31.25
QZT	62.07	37.93
QZN	55.17	44.83

## Molecular Dynamics Simulation

The study of metal corrosion in various conditions uses the crucial tool of molecular dynamic modeling [9,33]. To do this, molecular dynamics is used to determine how the investigated molecule will adsorb to the surface of the metal based on the adsorption or binding energies of the interaction between the metal surface and the inhibitor molecule [34]. Al(1 1 0) surfaces were used to model the inhibitors QZN, QZT and QZO due to the face's relatively dense atom population [35]. Modeling was done using FORCITE tools created in BIOVIA/Material studio 8.0. (Accelrys, Inc.).

In a simulation box of 17 Å x 12 Å x 28 Å with a periodic boundary condition, calculations were performed using the COMPASS force field and smart algorithm [2,10]. Figure 5 displays images of the molecules on the Al(1 1 0) surface in their side and top views with their lowest energy forms. This visually shows that the molecules have a flat-lying orientation on the surface of the metals due to their benzenoid structure and most of the atoms interact well with the metal surface.

Bond lengths and angles of the molecules can be utilized as indicators. They can be assessed before and after the molecule-metal interactions to further establish the contact of each molecule with the metals' surface [2]. The numbers reported in Tables 4a–c were taken from the molecular structures corresponding to each molecule's lowest energy after the quenched simulation from the results of the bond length evaluation obtained before and after the simulation of the molecules on the Al(1 1 0) surface. Except for the C<sub>5</sub>-C<sub>10</sub> and C<sub>8</sub>-C<sub>9</sub> bond lengths, it can be shown from Table 4a for QZN that most of the bond lengths were not changed during the adsorption of the molecule on the surface of Al(1 1 0).

In Table 4b, QZO, five bond lengths: N<sub>1</sub>-C<sub>2</sub>, C<sub>2</sub>-C<sub>3</sub>, N<sub>3</sub>-C<sub>4</sub>, C<sub>10</sub>-N<sub>1</sub> and C<sub>4</sub>-N<sub>12</sub> were all altered due to molecular contact with the metal's surface. Table

4c, which showed the bond lengths of QZT before and after adsorption on the metal, demonstrated that the molecular interaction caused all of the bond lengths in the molecule to alter. With the observation that the bond length of the molecules involved in the inhibition of Al(1 1 0) during the inhibition process, the bond length considerably changes. When compared to variations in the bond lengths of QZO and QZT, significant changes in either length for QZN were not noticed. This might be due to the free side chains of QZO and QZT molecules, making it easier for them to bind with the metal surface and interact with the surface atoms [15].

**Table 4a.** Variation in bond length of the QZN molecule before and after simulation

Bond type	Length before adsorption (Å)	Length after adsorption (Å)
N <sub>1</sub> -C <sub>2</sub>	1.331	1.331
C <sub>2</sub> -N <sub>3</sub>	1.334	1.334
N <sub>3</sub> -C <sub>4</sub>	1.345	1.345
C <sub>4</sub> -C <sub>5</sub>	1.379	1.379
C <sub>5</sub> -C <sub>10</sub>	1.400	1.401
C <sub>10</sub> -N <sub>1</sub>	1.356	1.356
C <sub>5</sub> -C <sub>6</sub>	1.427	1.427
C <sub>6</sub> -C <sub>7</sub>	1.386	1.386
C <sub>7</sub> -C <sub>8</sub>	1.402	1.402
C <sub>8</sub> -C <sub>9</sub>	1.393	1.392
C <sub>9</sub> -C <sub>10</sub>	1.366	1.366
C <sub>10</sub> -N <sub>1</sub>	1.356	1.356

**Table 4b.** Variation in bond length of the QZO molecule before and after simulation

Bond type	Length before adsorption (Å)	Length after adsorption (Å)
N <sub>1</sub> -C <sub>2</sub>	1.363	1.364
C <sub>2</sub> -N <sub>3</sub>	1.396	1.401
N <sub>3</sub> -C <sub>4</sub>	1.459	1.465
C <sub>4</sub> -C <sub>5</sub>	1.459	1.459
C <sub>5</sub> -C <sub>10</sub>	1.403	1.403
C <sub>10</sub> -N <sub>1</sub>	1.373	1.371
C <sub>2</sub> -O <sub>11</sub>	1.220	1.220
C <sub>4</sub> -N <sub>12</sub>	1.295	1.294
C <sub>7</sub> -Cl <sub>19</sub>	1.713	1.713

**Table 4c** Variation in bond length of the QZT molecule before and after simulation

Bond type	Length before adsorption (Å)	Length after adsorption (Å)
N <sub>1</sub> -C <sub>2</sub>	1.367	1.365
C <sub>2</sub> -N <sub>3</sub>	1.372	1.380
N <sub>3</sub> -C <sub>4</sub>	1.446	1.459
C <sub>4</sub> -C <sub>5</sub>	1.454	1.456
C <sub>5</sub> -C <sub>10</sub>	1.415	1.412
C <sub>10</sub> -N <sub>1</sub>	1.408	1.403
C <sub>2</sub> -S <sub>11</sub>	4.193	4.165
C <sub>4</sub> -N <sub>12</sub>	1.713	1.714
C <sub>7</sub> -Cl <sub>19</sub>	1.295	1.294

Since it is anticipated that the compounds will adopt a flat orientation on the Al(1 1 0) surface, all of the inhibitor molecules' bond angles are either  $\pm 120^\circ$ . This serves as more evidence that throughout the inhibition process, the inhibitor molecules exhibit  $sp^2$  hybridization with primarily p-orbitals on the surface of the metal [15]. Tables 5a (QZN), 5b (QZO) and 5c (QZT) further show that, when the bond angles before and after adsorption were compared for each of the compounds under study on Al(1 1 0) surfaces, all measured bond angles altered as a result of the adsorption. This is evidence of the interaction of the molecules' atoms with the metal's surface. For all of the molecules (QZN, QZO and QZT) investigated, the before and after simulation values of the molecules were not entirely planar, which suggested that the molecules might not have a flat orientation on the aluminium surface to maximize surface adsorption.

**Table 5a** Variation in the bond angle of QZN molecule before and after simulation

Bond Angle	Before adsorption (°)	After adsorption (°)
N <sub>1</sub> -C <sub>2</sub> -N <sub>3</sub>	126.067	126.008
C <sub>10</sub> -N <sub>1</sub> -C <sub>2</sub>	116.579	116.627
C <sub>2</sub> -N <sub>3</sub> -C <sub>4</sub>	118.193	118.215
N <sub>3</sub> -C <sub>4</sub> -C <sub>5</sub>	119.752	119.215
N <sub>1</sub> -C <sub>10</sub> -C <sub>9</sub>	117.109	117.137
C <sub>4</sub> -C <sub>5</sub> -C <sub>6</sub>	122.747	122.751
C <sub>6</sub> -C <sub>7</sub> -C <sub>8</sub>	120.065	120.131

**Table 5b** Variation in bond angle of QZO molecule before and after simulation

Bond Angle	Before adsorption (°)	After adsorption (°)
N <sub>1</sub> -C <sub>2</sub> -N <sub>3</sub>	119.815	120.065
N <sub>1</sub> -C <sub>2</sub> -O <sub>11</sub>	117.927	117.512
O <sub>11</sub> -C <sub>2</sub> -N <sub>3</sub>	122.258	122.422
C <sub>2</sub> -N <sub>3</sub> -C <sub>13</sub>	122.308	122.037
N <sub>3</sub> -C <sub>4</sub> -N <sub>12</sub>	121.366	121.912
C <sub>4</sub> -C <sub>5</sub> -C <sub>6</sub>	122.226	122.152
C <sub>5</sub> -C <sub>6</sub> -C <sub>7</sub>	122.827	122.859
C <sub>6</sub> -C <sub>7</sub> -Cl <sub>19</sub>	121.512	121.240

**Table 5c** Variation in the bond angle of QZT molecule before and after simulation

Bond Angle	Before adsorption (°)	After adsorption (°)
N <sub>1</sub> -C <sub>2</sub> -N <sub>3</sub>	123.314	124.229
N <sub>1</sub> -C <sub>2</sub> -S <sub>11</sub>	118.335	115.337
S <sub>11</sub> -C <sub>2</sub> -N <sub>3</sub>	118.335	120.131
C <sub>2</sub> -N <sub>3</sub> -C <sub>13</sub>	116.815	117.559
N <sub>3</sub> -C <sub>4</sub> -N <sub>12</sub>	122.134	122.948
N <sub>12</sub> -C <sub>4</sub> -C <sub>5</sub>	121.661	120.442
C <sub>6</sub> -C <sub>7</sub> -Cl <sub>19</sub>	121.673	121.856
C <sub>1</sub> -C <sub>7</sub> -C <sub>8</sub>	121.402	121.215

Results of the quenched dynamic simulation of each investigated molecule on Al(1 1 0) surface are shown in Table 6. When contrasted to the -100kcal/mol result above, it can be seen that all adsorption energies are negative and low, separating physical adsorption from chemical adsorption [11,21,33]. Figure 3 shows the simulated adsorbed molecules on Al(1 1 0) with the lowest configuration. Additionally, Table 6 revealed the calculated positive values of the binding energies of the interactions between each molecule and the metal surface. These numbers were positive and under 100 kcal/mol, indicating physical adsorption as the mechanism.

The sequence of these compounds' adsorption and binding energies is QZO>QZT>QZN, with QZN serving as the reference molecule and QZO possibly being more inhibitory than the others. This could be due to functional groups other than the amine functional group found on the

reference molecule, QZN, QZT and QZO. According to reports, pi-bonds and the relative size of the molecule also help in adsorption, which is why QZO and QZT adsorb more than QZN [34-36]. According to Umaru and Ayuba [31], compounds containing more functional groups or hetero atoms (such as QZO and QZT) are more adsorptive than those with fewer functional groups (QZN).

**Table 6.** Calculated molecular dynamic simulation parameters for the studied molecules

Properties (kcal/mol)	QZN	QZT	QZO
Total kinetic energy	10.892 ±5.03	15.291 ±0.92	16.158 ±2.287
Total potential energy	14.989 ±0.89	-125.867 ±1.17	-135.629 ±4.29
Energy of the molecule	46.637 ±0.09	-64.700 ±0.00	-73.703 ±0.00
Energy of the surface	0.000 ±0.00	0.000 ±0.00	0.000 ±0.00
Adsorption energy	-31.592 ±0.00	-61.174 ±0.00	-61.926 ±0.00
Binding energy	31.592 ±0.00	61.174 ±0.00	61.926 ±0.00

## Conclusion

Quantum chemical and molecular dynamic modeling techniques were employed to examine the corrosion prevention of aluminum metal surfaces utilizing three quinazoline derivatives. Quantum chemical calculations for the compounds under study showed that QZO is substantially more nucleophilic than the other two (QZT and QZN). The hetero atoms in these molecules were discovered to be the likely point of contact with the aluminum metal surface after these molecules' local and global reactivity indices were examined utilizing the Fukui technique. Each molecule's quenched molecular dynamic simulation on the Al(1 1 0) surface indicated that the interaction is caused by van

der Waals forces, which is a physical adsorption mechanism.

## Acknowledgment


The authors are grateful to Dr. Arthur Ebuka David, Department of Pure and Applied Chemistry, University of Maiduguri, Borno State, Nigeria, for the BIOVIA Materials Studio software.

## Disclosure statement

The authors reported no potential conflict of interest.

## ORCID

Fater Iorhuna : 0000-0002-1018-198X

Abdulfatah S. Muhammad : 0000-0002-4191-2749

Abdullahi M. Ayuba : 0000-0002-2295-8282

## References

- [1] S.C. Nwanonenyi, H.C. Obasi, I.O. Eze, *Chem. Africa*, **2019**, 2, 471–482. [[CrossRef](#)], [[Google Scholar](#)], [[Publisher](#)]
- [2] N. Raghavendra, *Chem. Africa*, **2020**, 3, 21–34. [[CrossRef](#)], [[Google Scholar](#)], [[Publisher](#)]
- [3] R.E. Melchers, T. Wells, *Corros. Eng. Sci. Technol.*, **2018**, 53, 524–530. [[CrossRef](#)], [[Google Scholar](#)], [[Publisher](#)]
- [4] T.F. Maryer, C. Gehlen, C. Deuberschmidt, *16-Corrosion monitoring in concrete*, In *Techniques for Corrosion Monitoring*, 2<sup>nd</sup> Edition, Woodhead publishing series in metals and surface engineering, **2021**, pp. 379–405. [[CrossRef](#)], [[Publisher](#)]
- [5] S.C. Udensi, O.E. Ekpe, L.A. Nnanna, *Chem. Africa*, **2020**, 3, 303–316. [[CrossRef](#)], [[Google Scholar](#)], [[Publisher](#)]



- [6] H. Lgaz, R. Salghi, A. Chaouiki, S. Shubhalaxmi, S. Jodeh, K.S. Subrahmanya, *Cogent Eng.*, **2018**, 5, 1441585. [[CrossRef](#)], [[Google Scholar](#)], [[Publisher](#)]
- [7] S. Jyothi, K. Rathidevi, *Rasayan J. Chem.*, **2017**, 10, 1253–1260. [[CrossRef](#)], [[Google Scholar](#)]
- [8] S. John, J. Joy, M. Prajila, A.J. Joseph, *Mater. Corros.*, **2011**, 62, 1031–1041. [[CrossRef](#)], [[Google Scholar](#)], [[Publisher](#)].
- [9] N.O. Eddy, P.O. Ameh, N.B. Essien, *J. Taibah Univ. Sci.*, **2018**, 12, 545–556. [[CrossRef](#)], [[Google Scholar](#)]
- [10] P.S. Neriyaana, V.D. Alva, *Chem. Africa*, **2020**, 3, 1087–1098. [[CrossRef](#)], [[Google Scholar](#)], [[Publisher](#)].
- [11] O.D. Ofuyekpone, O.G. Utu, B.O. Onyekpe, U.G. Unueroh, A.A. Adediran, *Chem. Africa*, **2022**, 17, 1–8. [[CrossRef](#)], [[Google Scholar](#)], [[Publisher](#)]
- [12] S.J. Smith, B.T. Sutcliffe, *Review in computational chemistry*, **2007**, pp. 271–316. [[CrossRef](#)], [[Publisher](#)].
- [13] S. Ouchenane, R. Jalgham, S. Rezgoun, H. Saifi, M. Bououdina, *Chem. Africa*, **2021**, 4, 621–633. [[CrossRef](#)], [[Google Scholar](#)], [[Publisher](#)]
- [14] G. Bereket, E. Hur, C. Ogretir, *J. Mol. Struct.*, **2002**, 578, 79–88. [[CrossRef](#)], [[Google Scholar](#)], [[Publisher](#)]
- [15] M.E. Belghiti, S. Echihi, A. Dafali, Y. Karzazi, M. Bakasse, H. Elalaoui-Elabdallaoui, *Appl. Surf. Sci.*, **2019**, 491, 707–722. [[CrossRef](#)], [[Google Scholar](#)], [[Publisher](#)]
- [16] I. Obot, Z. Gasem, S.A. Umoren, *Int. J. Electrochem. Sci.*, **2014**, 9, 2367–2378. [[Google Scholar](#)]
- [17] K.F. Khaled, *Electrochim. Acta*, **2008**, 53, 3484–3492. [[CrossRef](#)], [[Google Scholar](#)], [[Publisher](#)]
- [18] L. Guo, M. Zhu, J. Chang, R. Thomas, R. Zhang, P. Wang, *Int. J. Electrochem. Sci.*, **2021**, 16, 211139. [[CrossRef](#)], [[Google Scholar](#)]
- [19] H. Lgaz, S. Masroor, M. Chafiq, M. Damej, A. Brahmia, R. Salghi, *Constr. Build. Mater.*, **2020**, 10, 357. [[CrossRef](#)], [[Google Scholar](#)]
- [20] W. Kohn, A.D. Becke, R.G. Parr, *J. Phys. Chem.*, **1996**, 100, 12974–12980. [[CrossRef](#)], [[Google Scholar](#)], [[Publisher](#)]
- [21] O.E. Oyeneyin, N.D. Ojo, N. Ipinloju, A.C. James, E.B. Agbaffa, *Chem. Africa*, **2022**, 5, 319–332. [[CrossRef](#)], [[Google Scholar](#)], [[Publisher](#)]
- [22] H. Zhang, Y. Chen, Z. Zhang, *Result Phys.*, **2018**, 11, 554–563. [[CrossRef](#)], [[Google Scholar](#)], [[Publisher](#)]
- [23] M. Talari, S.M. Nezhad, S.J. Alavi, M. Mohtashamipour, A. Davoodi, S. Hosseinpour, *J. Mol. Liq.*, **2019**, 286, 110915. [[CrossRef](#)], [[Google Scholar](#)], [[Publisher](#)]
- [24] J. Frau, D. Glossman-Mitnik, *Front. Chem.*, **2017**, 5, 16. [[CrossRef](#)], [[Google Scholar](#)], [[Publisher](#)]
- [25] M. Belghiti, Y. El Ouadi, S. Echihi, A. Elmelouky, H. Outada, Y. Karzazi, *Surf. Interf.*, **2020**, 21, 100692. [[CrossRef](#)], [[Google Scholar](#)], [[Publisher](#)]
- [26] A. Dehghani, A.H. Mostafatabar, G. Bahlakeh, B. Ramezanzadeh, M. Ramezanzadeh, *J. Mol. Liq.*, **2020**, 309, 113035. [[CrossRef](#)], [[Google Scholar](#)], [[Publisher](#)]
- [27] A. Popova, M. Christov, S. Raicheva, E. Sokolova, *Corros. Sci.*, **2004**, 46, 1333–13350. [[CrossRef](#)], [[Google Scholar](#)], [[Publisher](#)]
- [28] C.B. Verma, M.A. Quraishi, A. Singh, *J. Taiwan Inst. Chem. Eng.*, **2015**, 49, 229–239. [[CrossRef](#)], [[Google Scholar](#)], [[Publisher](#)]
- [29] B. Gómez, N.V. Likhanova, M.A. Domínguez-Aguilar, R. Martínez-Palou, A. Vela, J.L. Gázquez, *J. Phys. Chem. B*, **2006**, 110, 8928–8934. [[CrossRef](#)], [[Google Scholar](#)], [[Publisher](#)]
- [30] M.A. Bedair, *J. Mol. Liq.*, **2016**, 219, 128–141. [[CrossRef](#)], [[Google Scholar](#)], [[Publisher](#)]
- [31] U. Umar, A.M. Ayuba, *RHAZES: Green Appl. Chem.*, **2020**, 10, 113–128. [[Google Scholar](#)], [[Publisher](#)]

- [32] L. Guo, Z.S. Safi, S. Kaya, W. Shi, B. Tüzün, N. Altunay, *Front. Chem.*, **2018**, 6, 155. [[CrossRef](#)], [[Google Scholar](#)], [[Publisher](#)]
- [33] S.Kaya, L. Guo, C. Kaya, B. Tu"zu"n, I.B. Obot, R. Tourir, *J. Taiwan Inst. Chem. Eng.*, **2016**, 65, 522–529. [[CrossRef](#)], [[Google Scholar](#)], [[Publisher](#)]
- [34] TV. Kumar, J. Makangara, C. Laxmikanth, N.S. Babu, NS, *Int. J. Comput. Theor. Chem.*, **2016**, 4, 1–6. [[CrossRef](#)], [[Google Scholar](#)], [[Publisher](#)]
- [35] G.M. Al-Mazaideh, T.S. Ababneh, K.H. Abu-Shandi, R. Jamhour, H.A. Salman, A.M. Al-Msiedeen, *Phys. Sci. Int. J.*, **2016**, 12, 1–7. [[CrossRef](#)], [[Google Scholar](#)], [[Publisher](#)]
- [36] K. Khaled, N. Abdel-Shafi, N.A. Al-Mobarak, *Int. J. Electrochem. Sci.*, **2012**, 7, 1027–1044. [[Google Scholar](#)]

#### HOW TO CITE THIS ARTICLE

Fater Iorhuna, Adulfatah Shehu Muhammad, Abdullahi Muhammad Ayuba. Quinazoline Derivatives as Corrosion Inhibitors on Aluminium Metal Surface: A Theoretical Study. *Adv. J. Chem. A*, **2023**, 6(1), 71-84.

DOI: [10.22034/AJCA.2023.370123.1347](https://doi.org/10.22034/AJCA.2023.370123.1347)

URL: [http://www.ajchem-a.com/article\\_163138.html](http://www.ajchem-a.com/article_163138.html)